Ann. Geophys., 26, 3731–3739, 2008
www.ann-geophys.net/26/3731/2008/

Annales Geophysicae

Influence of gravity waves and tides on mesospheric temperature inversion layers: simultaneous Rayleigh lidar and MF radar observations

S. Sridharan[1], **S. Sathishkumar**[2], **and S. Gurubaran**[2]

[1]National Atmospheric Research Laboratory, Gadanki-517 112, Pakala Mandal, Chittoor, India
[2]Equatorial Geophysical Research Laboratory, Indian Institute of Geomagnetism, Krishnapuram, Tirunelveli-627 011, India

Received: 24 March 2008 – Revised: 20 October 2008 – Accepted: 21 October 2008 – Published: 25 November 2008

Abstract. Three nights of simultaneous Rayleigh lidar temperature measurements over Gadanki (13.5° N, 79.2° E) and medium frequency (MF) radar wind measurements over Tirunelveli (8.7° N, 77.8° E) have been analyzed to illustrate the possible effects due to tidal-gravity wave interactions on upper mesospheric inversion layers. The occurrence of tidal gravity wave interaction is investigated using MF radar wind measurements in the altitude region 86–90 km. Of the three nights, it is found that tidal gravity wave interaction occurred in two nights. In the third night, diurnal tidal amplitude is found to be significantly larger. As suggested in Sica et al. (2007), mesospheric temperature inversion seems to be a signature of wave saturation in the mesosphere, since the temperature inversion occurs at heights, when the lapse rate is less than half the dry adiabatic lapse rate.

Keywords. Atmospheric composition and structure (Pressure, density, and temperature) – Meteorology and atmospheric dynamics (Middle atmosphere dynamics; Waves and tides)

1 Introduction

Temperature inversions have been ubiquitous features in the mesosphere and lower thermosphere (MLT) region. They have been studied by several authors in the past few decades and most of the important findings are recently reviewed by Meriwether and Gardner (2000) and Meriwether and Gerrard (2004). They are found to occur more frequently in winter months at mid-latitudes (Leblanc and Hauchecorne, 1997) and in equinox months in low-latitudes (Siva Kumar et al., 2001). The mid-latitude observations show that they are longitudinally extended phenomena and are not local. There are different schools of thought on how these inversions are formed. Whiteway (1995) suggested that the inversions could be formed due to turbulent mixing. Hauchecorne et al. (1987) suggested that the inversions were due to gravity waves breaking within the inversion region for extended periods. The peak altitudes of mesospheric inversion layer (MIL) events will often show a downward phase progression typical of the diurnal tide. States and Gardner (2000) showed that the inversion layer could not be observed in the 24-h averaged sodium resonance lidar observations suggesting the role of diurnal tide or its sub harmonics. However, the amplitude of mesospheric inversion is considerably greater than tidal model predictions attributed to migrating tidal waves alone. Both the NCAR general circulation model and the Global Scale Wave Model predicted similar and smaller amplitudes than the observed. Meriwether et al. (1998) suggested that the enhancement of the MIL amplitude to temperatures considerably elevated above that represented by the tidal structure alone may be indicative of dynamical forcing. A possible source for this was suggested to be gravity waves interacting with tidal wave activity. Liu et al. (2000)'s model calculations showed that the breaking of a gravity wave with a 50 km horizontal wavelength and a horizontal phase speed of 30 ms^{-1} could cause downward propagating MIL. The other possible mechanism for the occurrences of these inversions with large amplitudes could be due to chemical heating through exothermic reactions as reported by Meriwether and Mlynczak (1995).

Using coincident measurements with the MF radar and lidar at Western Ontario (42.9° N, 81.4° W), Sica et al. (2002) observed that there are two type of inversions. The first type, which persists for many hours, is associated with increased gravity wave variance, as the magnitude of westward tide decreases. The second type of inversion persists for less than 2 h, but the increase in temperature, is much greater than that expected from tidal dissipation. Using Canadian Middle

Correspondence to: S. Sridharan
(ssri_dhar@rediffmail.com)

Published by Copernicus Publications on behalf of the European Geosciences Union.

atmosphere Model (CMAM), Sica et al. (2007) predicted that the environmental lapse rate must be less than half the adiabatic lapse rate for an inversion to form, and it predicts the ratio of the inversion amplitude and thickness as a function of environmental lapse rate.

Though there have been a lot of studies on mesospheric inversions (see review article by Meriwether and Gerrard, 2004), the formation mechanisms of the mesospheric inversions have not yet been understood. In the present study, three nights of simultaneous measurements with the MF radar zonal wind observations over Tirunelveli (8.7° N, 77.8° E) and Rayleigh lidar temperature observations over Gadanki (13.5° N, 79.2° E) are presented and discussed to illustrate the possible effects due to tidal-gravity wave interactions on upper mesospheric inversion layers. As suggested by Sica et al. (2007), the mean temperature profiles are compared with the dry adiabatic lapse rate profiles to see whether the condition "environmental lapse rate less than dry adiabatic lapse rate" is satisfied for the formation of mesospheric inversion.

2 Data analysis

2.1 Rayleigh lidar temperature measurements

The Rayleigh lidar system at National Atmospheric Research Laboratory, Gadanki employs the second harmonic of Nd:YAG pulsed laser at 532 nm with an energy of about 550 mJ at a pulse repetition rate of 20 Hz and a pulse width of 7 ns. The Rayleigh lidar technique involves range resolved detection of molecular backscattered laser radiation from altitudes above 30 km, where the atmosphere is free from aerosols. The Rayleigh receiver employs a Newtonian telescope of diameter 750 mm, detected by photo multiplier and counted sequentially into successive 300-m range bins. More details of this instrument and method of analysis can be had from Siva Kumar et al. (2003). The four minute averaged photon count profiles were averaged for 30 min and temperature and its standard error are determined using the method given by Hauchecorne and Chanin (1980).

The relative density is calculated from the number of photons backscattered ($N(z)$), by a layer of thickness Δz at altitude z assuming (i) the scattering due to aerosols is negligible compared to molecular scattering, (ii) the atmospheric transmission is constant throughout the entire zone and (iii) the telescope field of view is large enough to include the entire volume of the scattered beam, using the following relation (Keckhut et al., 1993)

$$\rho(z) = \frac{C(z - z_o)^2 N(z)}{\Delta z},$$

where C is the normalizing constant, which is altitude independent and Δz is the vertical spatial resolution (300 m). The constant C is determined by taking CIRA 86 model density values at 40 km and the absolute density profile is derived. The uncertainty on the density profile is assumed to be equal to the statistical standard error

$$\frac{\delta\rho(z)}{\rho(z)} = \frac{|N(z) + N_m|^{1/2}}{N(z)}$$

where $\delta\rho(z)$ is the standard deviation of atmospheric density and N_m is the background noise. All subsequent quantities are derived from the density profile and the corresponding error bars are calculated from Gaussian error propagation (Schöch, 2007; Schöch et al., 2008).

The pressure profile is computed from the density profile assuming the atmosphere to be in hydrostatic equilibrium. The temperature profile $T(z_i)$ is derived from pressure and density profile assuming that the atmosphere obeys ideal gas law and is expressed as:.

$$T(z_i) = \frac{Mg(z_i)\Delta z}{R\mathrm{Log}(1+X)}, \quad \text{where} \quad X = \frac{\rho(z_i)g(z_i)\Delta z}{P(z_i + \Delta z/2)}$$

The statistical standard error on the temperature is

$$\frac{\delta T(z_i)}{T(z_i)} = \frac{\delta\left[\mathrm{Log}(1+X)\right]}{\mathrm{Log}(1+X)} = \frac{\delta X}{(1+X)\mathrm{Log}(1+X)}$$

with

$$\left(\frac{\delta X}{X}\right)^2 = \left|\frac{\delta\rho(z_i)}{\rho(z_i)}\right|^2 + \left|\frac{\delta P(z_i + \Delta z/2)}{P(z_i + \Delta z/2)}\right|^2$$

$$\delta P(z_i+\Delta z/2)^2 = \sum_{j=i+1}^{n} \left|g(z_j)\delta\rho(z_j)\Delta z\right|^2 + |\delta P_m(z_n+\Delta z/2)|^2$$

$$P(z_i + \Delta z/2) = \sum_{j=i+1}^{n} g(z_j)\rho(z_j)\Delta z + P_m(z_n + \Delta z/2),$$

where $P(z_i+\Delta z/2)$ is the pressure at the top of the i-th layer and P_m is the pressure of the topmost layer upto which density profile is calculated (90 km). The value of P_m is taken from CIRA 86 model atmosphere.

The temperatures determined for every 30 min are averaged for the entire night and are further smoothed vertically by 10 points (3 km) to obtain a mean temperature profile. Atmospheric internal gravity waves are observed in profiles of fractional temperature perturbation, $T'(z)/T_o(z)$, Perturbations, $T'(z)=T(z)-T_o(z)$, are extracted from half-hour average temperature profiles by approximating an unperturbed background state (Whiteway et al., 1995).

Profiles of mean square perturbations and available potential energy density are determined from the variance of temperature fluctuations. As done by Tsuda et al. (2000), the variance $\overline{T'(z)}^2$ of the temperature fluctuations is calculated from the series of half-hour averaged temperature profiles obtained on a given night as

$$\overline{T'(z)}^2 = \frac{1}{Z_{\max} - Z_{\min}} \int_{Z\,\min}^{Z\,\max} T'^2 dz$$

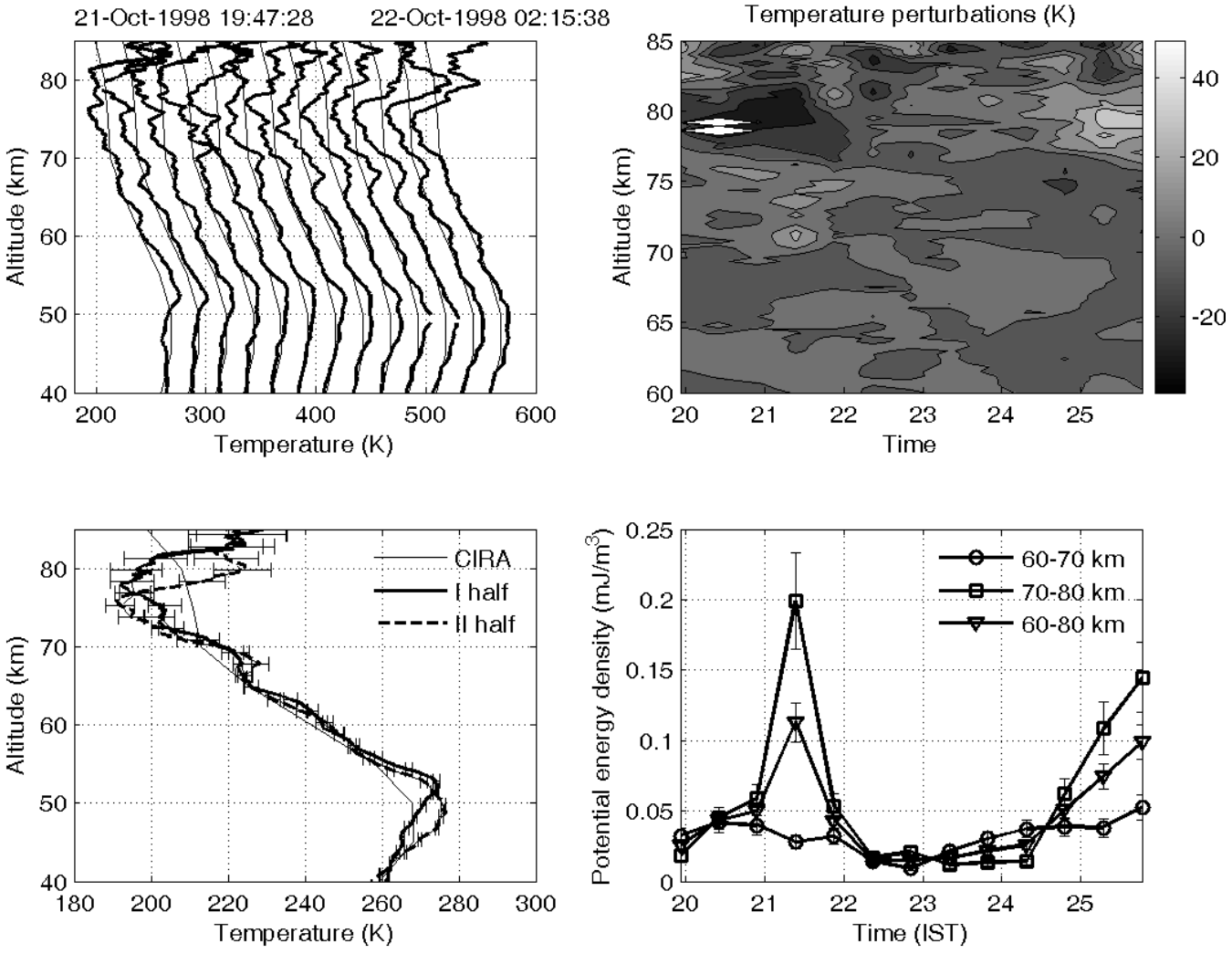

Fig. 1. **(a)** Sequence of altitude profiles of temperature (top left), **(b)** temperature profiles averaged for the first and second half of the observation period (bottom left), **(c)** contour plot showing temperature perturbations from the night mean profile (top right) and **(d)** time variation of potential energy averaged for 60–70 km, 70–80 km and 60–80 km for 21–22 October 1998 (bottom right).

As suggested in Whiteway et al. (1995), the computed variance may have a component due to noise fluctuations in the photon counting process and is subtracted to obtain an accurate measure of the associated available potential energy, which is given by

$$Ep(z) = \frac{1}{2}\left(\frac{g}{N(z)}\right)^2 \left(\frac{\overline{T'(z)}}{T_0(z)}\right)^2$$

within a layer with top and bottom layer heights $Z_{\max}$ and $Z_{\min}$ respectively (Tsuda et al., 2000). The variance at a given altitude is determined for a layer of 3 km thick, by sliding both top and bottom height of the layer with a step of 300 m. The brunt-Vaisala frequency squared, N^2 is calculated by differentiating the mean temperature profile with adjacent three heights (Tsuda et al., 2000). The error in the estimation of brunt-Vaisala frequency squared and potential energy per unit volume is below 10% at heights below 50 km. It increases to 10–30% at heights 60–75 km and to even 50% at heights above 80 km. The available potential energy per unit volume is determined by multiplying the above equation by the mean density profiles of the entire observation period on the night.

2.2 MF radar measurements

The MF radar (1.98 MHz) at Tirunelveli (8.7° N, 77.8° E) has been installed and operated by Indian Institute of Geomagnetism since November 1992 (Rajaram and Gurubaran, 1998). It provides horizontal wind information in the altitude region 68–98 km for every 2 km height interval and 2 min time interval. The pulse width of 30 μs limits the height resolution to 4.5 km. The raw winds are available every 2 min.

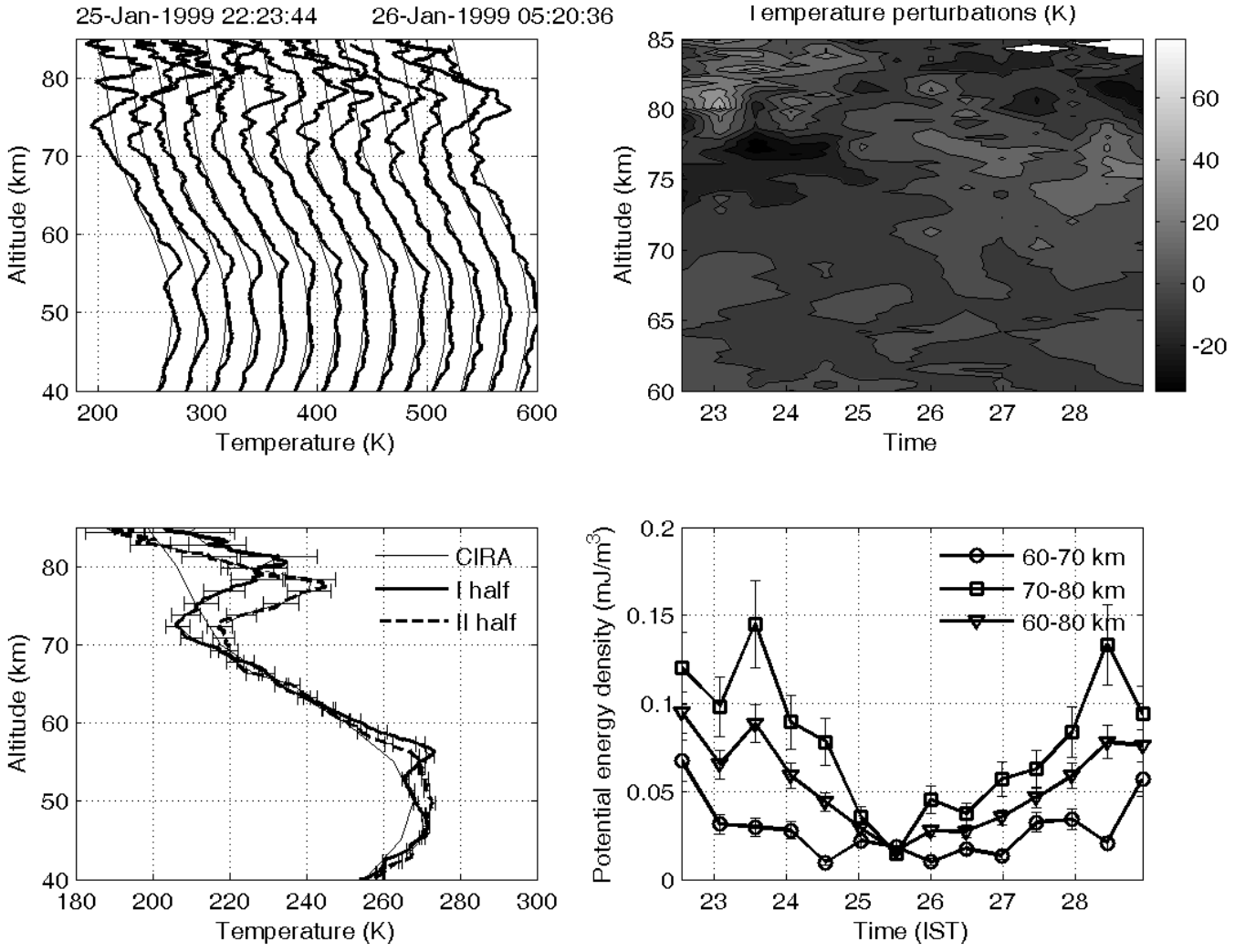

Fig. 2. Same as Fig. 1 except that it is for 25–26 January 1999.

For the present study, the zonal wind data for a bandwidth of 4 days centred on the days cosidered for Rayleigh temperature measurements are chosen. These four day data set are fitted with 24 h, 12 h and 8 h components and the time variation of each tidal components are obtained. The raw measurements in the 86–90 km height range at 2 km intervals are used to obtain wind fluctuations variances in each 1 h and they are correlated with the time variation of tidal components. This method is similar to the one described in Thayaparan et al. (1995).

3 Results

3.1 Mesospheric temperature inversion

3.1.1 21–22 October 1998

The left panels of Fig. 1 show sequence of temperature profiles (top panel) and the temperature profile averaged for first and second halves of the observation period (bottom panel) for the night of 21–22 October 1998 and for the altitude region 40–90 km. An upper mesospheric inversion layer is evident in the second half of the night (dashed line in the bottom figure). Below this region the lapse rates in both first and second halves are much steeper than the value expected from CIRA-86 model values (plotted as thin line). The top right panel of Fig. 1 shows the temperature variations from the mean changes in temperature as a function of height and time. The mesospheric inversion occurs during the second half of the measurement period, where between 78 and 82 km

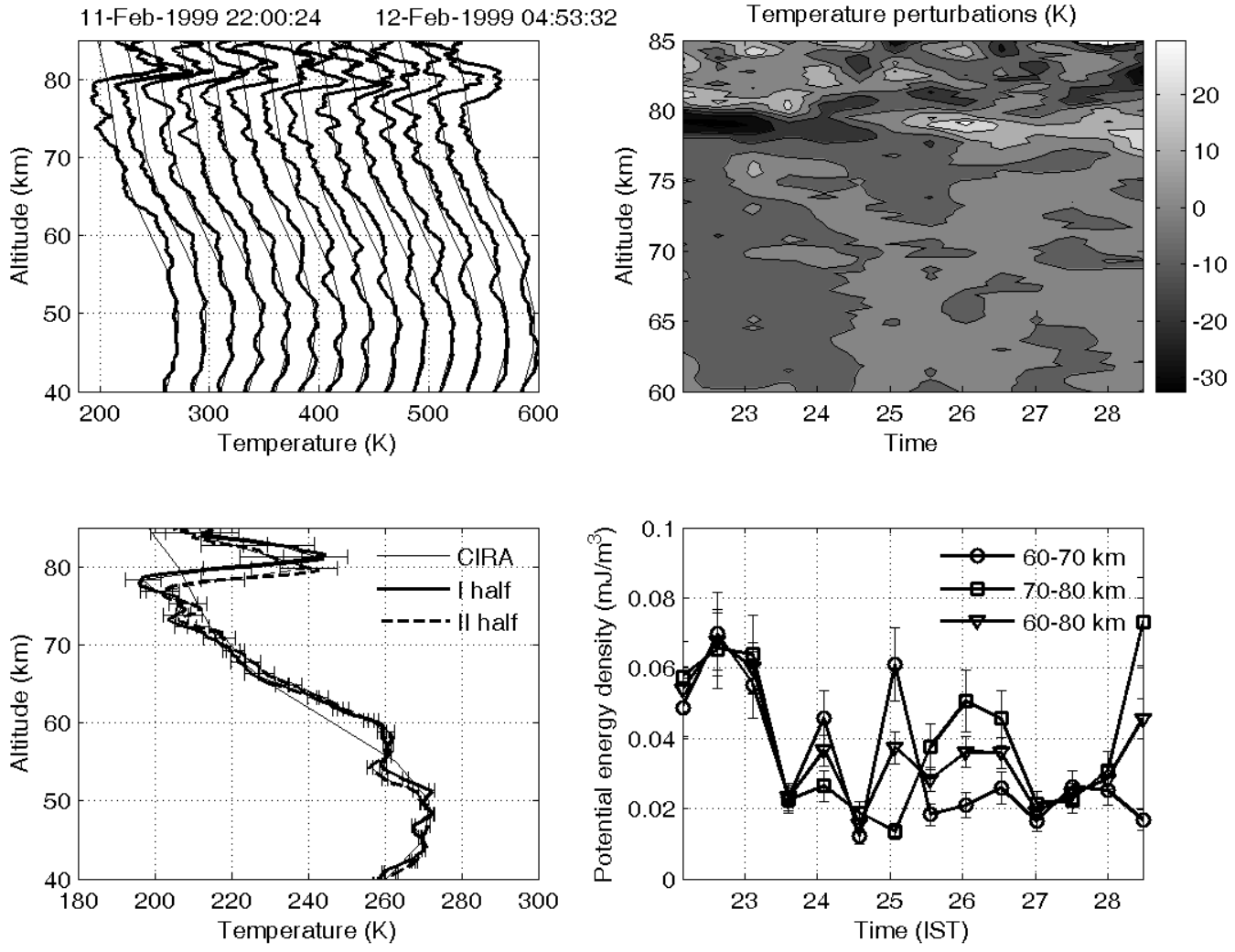

Fig. 3. Same as Fig. 1 except that it is for 11–12 February 1999.

the average temperature is 15–30 K higher when compared to the first half. Above the region of warming, there is a significant cooling of similar magnitude (15–30 K).

The total gravity wave potential energy density for the upper mesosphere is shown in the right bottom panel of Fig. 1. After 2230 h, the mesospheric potential energy densities in the altitude region (60–70 km) increase in concert with the temperature in the inversion region. They show larger values during the time (20:00–22:00 IST) of extended cooling also.

3.1.2 25–26 January 1999

In this case, temperature inversion occurs for a shorter time in the first half of the observation period (Fig. 2). In the second half of the observation period, the inversion occurs at lower height. Though the averaged temperature profile shows that the temperature inversion amplitude is smaller in the first half than in the second half, the time variation of temperature from the mean shows the inversion occurred for a shorter time in the first half, but with a warming greater than 40 K. Below this warming, there is a cooling greater than 20 K. After 2500 h, warming prevails, however, with smaller amplitude than in the first half of the observation period, till the end of the observation period. Above the region of extended warming, cooling is observed.

The potential energy density per unit volume for the height region 60–70 km shows larger values in the beginning and end of the observation period, when the inversion amplitude is larger. The total gravity wave kinetic energy density is weaker from 2530 h to the end of the observation period.

3.1.3 11–12 February 1999

In this case, temperature inversion occurred during 2200–2500 h just above 80 km. There exists cooling by about 20 K just below 80 km (Fig. 3). However, after 2500 h, the inversion occurs at still lower region. During the entire observation period, the maximum amplitude of the inversion

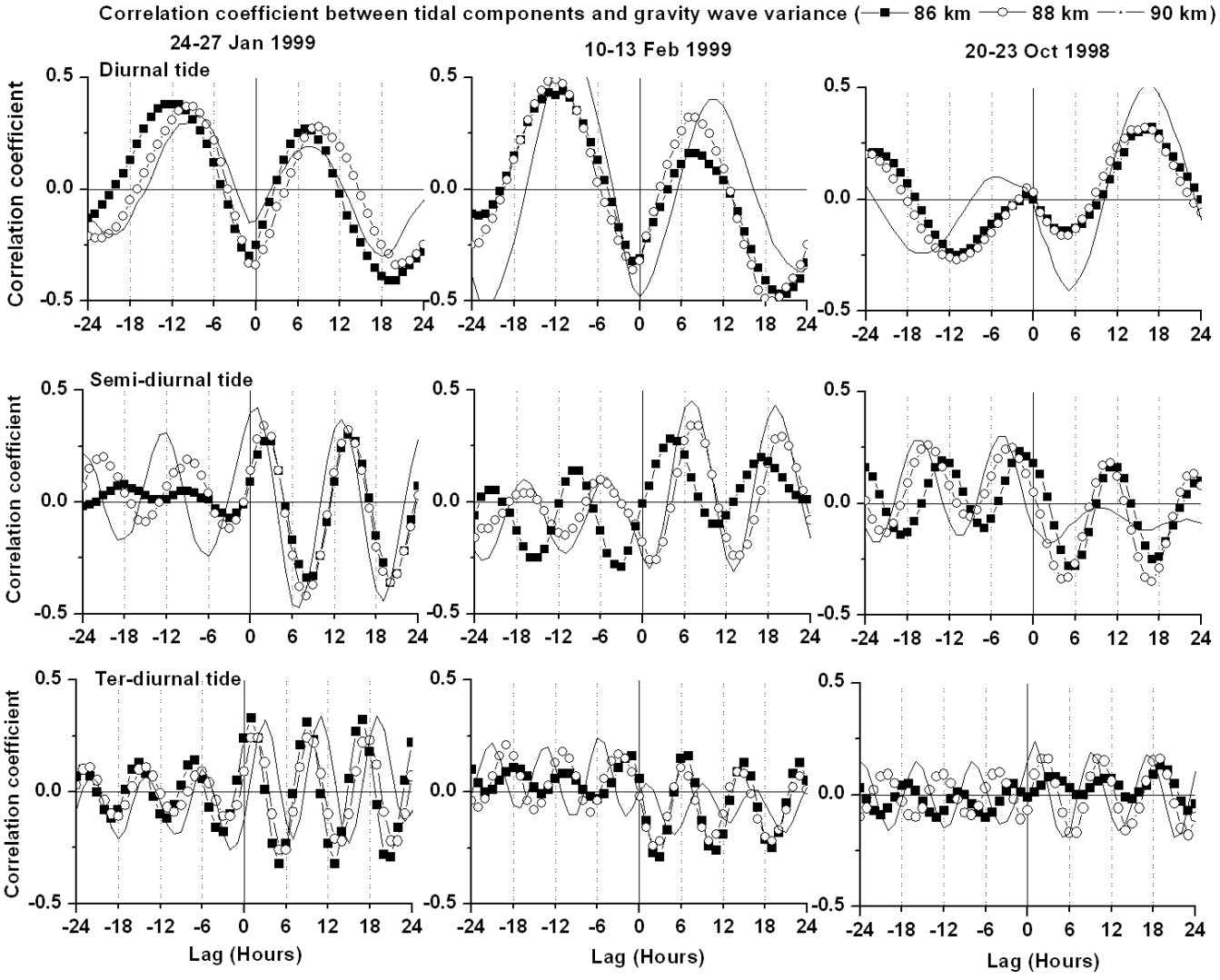

Fig. 4. Correlation coefficient between tidal components and gravity wave variances in zonal winds at 86–90 km.

occurred around 2600 h. Though the gravity wave potential energy density for the height region 60–70 km shows larger values for the temperature inversion occurred just above 80 km during 2200–2500 h, it shows minimum values from 2530 h to the end of the observation period.

3.2 Gravity wave tidal interaction

As mentioned in Sect. 2.2, the raw wind measurements (2 min) in the 86–94 km height range at 2 km intervals observed by MF radar at Tirunelveli are used to obtain wind fluctuations in each 1 h and they are correlated with the time variation of tidal components. Figure 4 shows the cross correlation coefficient between gravity wave variance and tidal components for 24–27 January 1999 (left panels), 10–13 February 1999 (middle panels) and 20–23 October 1998 (right panels). From the right panels of the figure, it can be inferred that the tidal components are not correlated with the gravity wave variance for 21–22 October 1998, as the correlation coefficient is nearly zero at zero lag. This suggests that the gravity wave tidal interaction does not occur. However, it may be noted that the diurnal tidal amplitude is significantly larger (40 m/s). Recently, Liu et al. (2007) found that when diurnal and semi-diurnal tidal amplitudes increase by factors of 2–3, a strong temperature inversion was observed around 90 km. The authors suggested that the temperature inversions occurring in a global scale were probably as a consequence of tidal planetary wave interaction. The nightly variations of three tidal components (diurnal, semi-diurnal and ter-diurnal) at 86 km are shown in the top (25–26 January 1999), middle (21–22 October 1999) and bottom (11–12 February 1999) panels of Fig. 5. On 21–22 October 1998, the semi diurnal (12 h) tide is positive (eastward) at the time extended cooling and crosses zero, when temperature is

around zero and reaches negative maxima (westward), when temperature shows larger warming. As the semi-diurnal tides are having large vertical wavelengths, we can assume that almost similar time variation is prevailing at the height of temperature inversions also. It suggests that the temperature change in the inversion region could be correlated with the semidiurnal tidal variation.

For the case of 24–27 January 1999, there exists anti-correlation between tidal components and gravity wave variances (left panels of Fig. 4). The correlation coefficient between these two is between -0.3– -0.4 at heights 88–94 km. On 10–13 February 1999, the correlation analysis between gravity wave variances and tidal components at upper mesospheric heights show the correlation coefficient of -0.5 at heights 90 and 92 km (middle panels of Fig. 4). It is interesting to note that ter-diurnal tidal amplitude is larger than semi-diurnal tidal amplitude. The comparison between the occurrence of MIL with the time variation of tidal components shows that the zero crossing of semi-diurnal tide coincides with the transition of cooling to warming at heights just below 90 km (middle panel of Fig. 5).

3.3 Relation between mesospheric inversion and dry adiabatic lapse rate

Recently, Sica et al. (2007) suggested that mesospheric temperature inversions can be formed, if the environmental lapse rate is less than half of the adiabatic lapse rate. We tested this condition on the mean temperature profiles for the nights 21–22 October 1998, 25–26 January 1999 and 11–12 February 1999. Figure 6 shows altitude variation of temperature lapse rate and mean temperature. The standard deviation of the lapse rate is below 2–3 km/h at heights below 70 km. In the height region 70–85 km, it increased from 3 km/h to 7 km/h with height. The adiabatic lapse rate is approximately 9.8 K/km and the half of it is 4.9 K/km. On 21–22 October 1998, mean temperature begins to decrease from the height 76 km to 80 km. It is nearly constant between 80 and 82 km. Again, it increases with height above 82 km. The background lapse rate (Γ) is much less the half of the adiabatic lapse rate ($\Gamma_a/2$) between the heights 72 km to 82 km to enable the inversion to be formed. On 25–26 January 1999, the mean temperature increases from about 73 km to 78 km. Again, coinciding with the rise in temperature, the Γ is much less than $\Gamma_a/2$ from 74 to 78 km. On 11–12 February 1999 also, coinciding with the increase in mean temperature, Γ is less than $\Gamma_a/2$. Inversions come back to normal at 82 km (11–12 February 1999) and 84 km (25–26 January 1999), when the lapse rate increases above half of the adiabatic lapse rate. If the background lapse rate is too large, then a saturated wave does not lead to an inversion. If it is less than half of dry adiabatic lapse rate, then a saturated wave may result in an inversion layer (Sica et al., 2007).

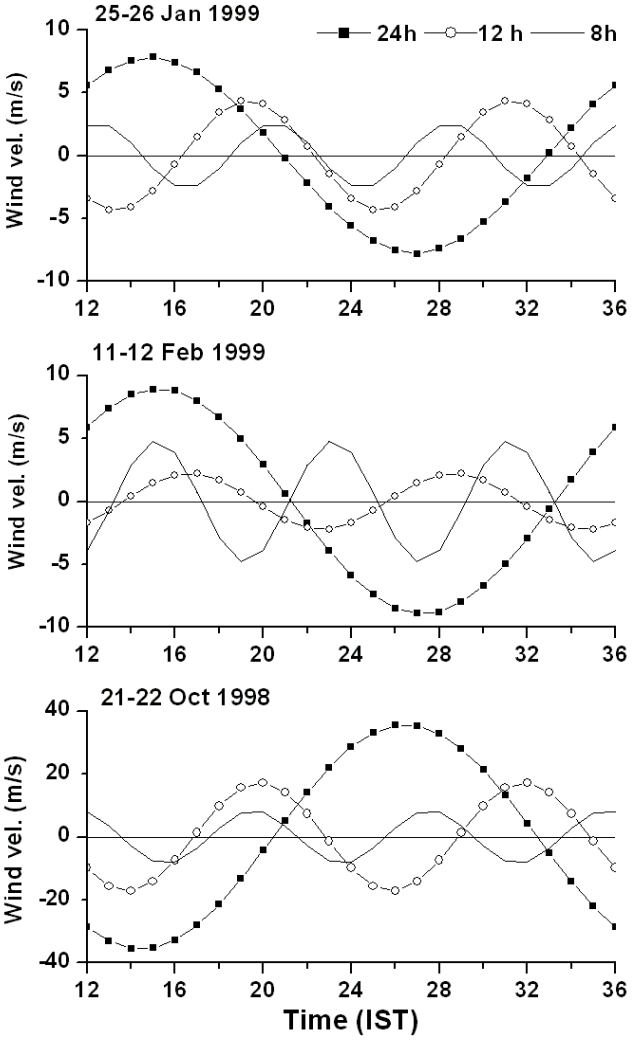

Fig. 5. Time variation of tidal components at 86 km on 25–26 January 1999 (top panel), 11–12 February 1999 (middle panel) and 21–22 October 1998 (bottom panel).

4 Discussion and conclusion

Simultaneous observations with the MF radar and Rayleigh lidar on three nights are presented to show the occurrence of mesospheric temperature inversions in the mesosphere region. Our observations do not always suggest direct relationship between inversion layers and gravity wave potential energy computed from temperature perturbations at or below the temperature inversion heights. The temperature variation seems to be correlated with that of the semi-diurnal tide. Since the semi-diurnal tide has large vertical wavelength, direct comparison between 90 km and lower mesospheric heights (80 km) is reasonable. The results shown in the present study reveals that there is an evidence for the occurrence of gravity wave-tidal interaction. A notable anti-correlation between the gravity wave variance and the amplitude of the diurnal tidal motion is clearly apparent for

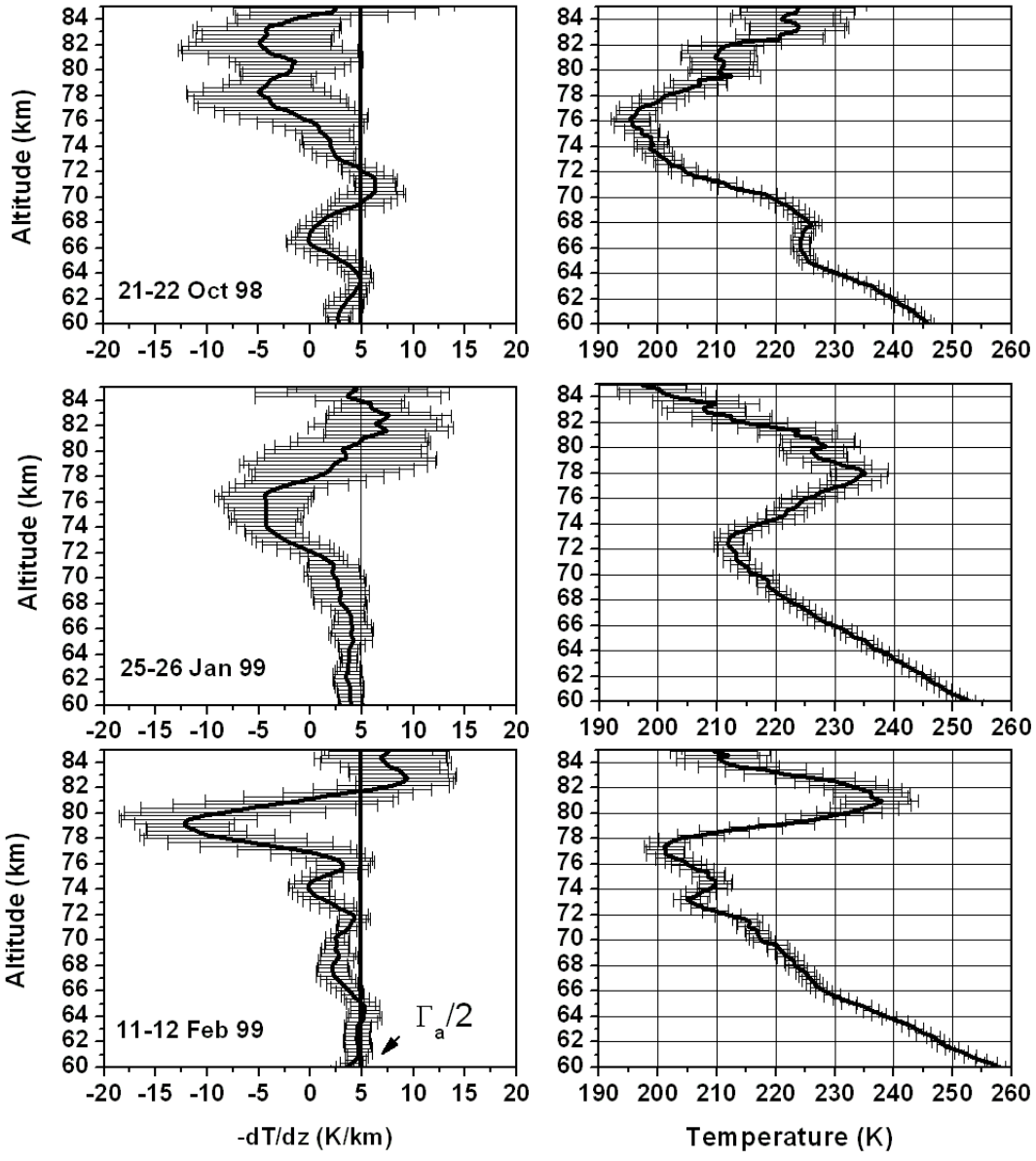

Fig. 6. The altitude variations of local environmental lapse rate (left panels) and mean temperature (right panels) over Gadanki. The uncertainties in the estimations are shown as error bars.

the zonal component. It occurs in phase at all four adjacent heights between 86–90 km, with similar correlation values. The gravity wave variance shows positive correlation with semi-diurnal tide. These observations showed that propagating gravity waves with periods less than 1 h can significantly modulate the tidal amplitudes, and the reverse is also true. Thayaparan et al. (1995) observed positive (negative) correlation between diurnal tidal amplitude and gravity wave variance in winter (summer) and observed no correlation between semidiurnal tidal amplitude and gravity wave variance. Sica et al. (2002) found positive correlation between semidiurnal tide and gravity wave variance. These observations suggest that gravity wave tidal interaction occurred.

Our observations show that cooling is observed above or below the warming region. During gravity wave breaking, heating rates are determined by wave advection, turbulent diffusion, and turbulence dissipative heating. Liu et al. (2000), through a series of numerical experiments, showed that the total heating rates could be large and could cause large local temperature changes. The wave advection could cause dynamical cooling in most of the wave breaking region. The simulation results showed that the large temperature changes in this process could form temperature inversion layers progressing downward with a speed similar to that of a diurnal tide phase speed, which clearly suggested the tidal modulation of the gravity wave and mean flow interactions.

Such a process is dependent on season and latitude, because the background state stability varies with season and latitude. The development of the temperature inversion is also affected by the gravity wave characteristics. Our observations show that the tidal-gravity wave interactions seem to occur in two of the three nights, as there is a correlation between gravity wave variance and diurnal tidal oscillation. In the other event, diurnal tidal amplitude is significantly larger. Liu et al. (2007) found when diurnal and semi-diurnal tidal amplitudes increase by factors of 2–3, a strong temperature inversion was observed around 90 km. The authors suggested that the temperature inversions occurring in a global scale are probably as a consequence of tidal planetary wave interaction.

Sica et al. (2007) suggested that mesospheric temperature inversions could be formed, if environmental lapse rate is less than half the adiabatic lapse rate. Our observations show that when there is an increase in temperature, the background lapse rate is much less than half the adiabatic lapse rate. The mean temperature decreases, whenever there is a large deviation from the dry adiabatic lapse rate. These results suggest that the mesospheric temperature inversion is a signature of wave saturation and the saturated wave can be gravity waves, tides or planetary waves.

Acknowledgements. This work is supported by Department of Space, Government of India. The authors would like to acknowledge the support of the operating staff in conducting Nd:YAG lidar experiments at NARL, Gadanki. The MF radar at Tirunelveli has been installed and operated by Indian Institute of Geomagnetism. The authors would like to thank the Topical Editor and the two anonymous referees for their critical evaluation of the manuscript.

Topical Editor U.-P. Hoppe thanks J. Meriwether and another anonymous referee for their help in evaluating this paper.

References

Hauchecorne, A. and Chanin, M. L.: Density and temperature profiles obtained by lidar between 35 and 70 km, Geophys. Res. Lett., 7, 565–568, 1980.

Hauchecorne, A., Chanin, M. L., and Wilson, R.: Mesospheric temperature inversion and gravity wave dynamics, Geophys. Res. Lett., 14, 935–939, 1987.

Leblanc, T. and Hauchecorne, A.: Recent observations of mesospheric temperature inversions, J. Geophys. Res., 102, 19 471–19 482, 1997.

Liu, H.-L., Hagan, M. E., and Roble, R. G.: Local mean state changes due to gravity wave breaking modulated by the diurnal tide, J. Geophys. Res., 105, 12 381–12 396, 2000.

Liu, H.-L., Li, T., She, C.-Y., Oberheide, J., Wu, Q., Hagan, M. E., Xu, J., Roble, R. G., Mlynczak, M. G., and Russell III, J. M.: Comparative study of short-term diurnal tidal variability, J. Geophys. Res., 112, D18108, doi:10.1029/2007JD008542, 2007.

Keckhut, P., Hauchecorne, A., and Chanin, M. L.: A critical review of the database acquired for the long-term surveillance of the middle atmosphere by the French Rayleigh lidars, J. Atmos. Ocean. Technol., 10, 850–867, 1993.

Meriwether, J. W. and Gardner, C. S.: A review of the mesosphere inversion layer phenomenon, J. Geophys. Res., 105, 12 405–12 416, 2000.

Meriwether, J. W. and Mlynczak, M. G.: Is chemical heating a major cause of the mesosphere inversion layer?, J. Geophys. Res., 100, 1379–1387, 1995.

Meriwether, J. W., Gao, X., Wickwar, V. B., Wilkerson, T., Beissner, K., Collins, S., and Hagan, M. E.: Observed coupling of the mesosphere inversion layer to the thermal tidal structure, Geophys. Res. Lett., 25, 1479–1482, 1998.

Meriwether, J. W. and Gerrard, A. J.: Mesosphere inversion layers and stratosphere temperature enhancements, Rev. Geophys., 42, RG3003, doi:10.1029/2003RG000133, 2004.

Rajaram, R. and Gurubaran, S.: Seasonal variabilities of low latitude mesospheric winds. Ann. Geophys., 16, 197–204, 1998, http://www.ann-geophys.net/16/197/1998/.

Sica, R. J., Thayaparan, T., Argall, P. S., Russell, A. T., and Hocking, W. K.: Modulation of upper mesospheric temperature inversions due to tidal-gravity wave interactions, J. Atmos. Sol.-Terr. Phys., 64, 915–922, 2002.

Sica, R. J., Argall, P. S., Shepherd, T. G., and Koshyk, J. N.: Model-measurement comparison of mesospheric temperature inversions, and a simple theory for their occurrence, Geophys. Res. Lett., 34, L23806, doi:10.1029/2007GL030627, 2007.

Schöch, A.: Thermal structure and gravity waves in the Arctic middle atmosphere above ALOMAR (69.3° N, 16.0° E), PhD thesis, Universität Rostock, Rostock, Germany, available at http://www.iap-kborn.de/Thesis-Master-Diploma-PhD.64.0.html?&L=1, 2007.

Schöch, A., Baumgarten, G., and Fiedler, J.: Polar middle atmosphere temperature climatology from Rayleigh lidar measurements at ALOMAR (69° N), Ann. Geophys., 26, 1681–1698, 2008, http://www.ann-geophys.net/26/1681/2008/.

Siva Kumar, V., Bhavani Kumar, Y., Raghunath, K., Rao, P. B., Krishnaiah, M., Mizutani, K., Aoki, T., Yasui, M., and Itabe, T.: Lidar measurements of mesospheric temperature inversion at a low latitude, Ann. Geophys., 19, 1039–1044, 2001, http://www.ann-geophys.net/19/1039/2001/.

Siva Kumar, V., Rao, P. B., and Krishnaiah, M.: Lidar measurements of stratosphere-mesosphere thermal structure at a low latitude: Comparison with satellite data and models, J. Geophys. Res., 108(D11), 4342, doi:10.1029/2002JD003029, 2003.

States, R. J. and Gardner, C. S.: Influence of the diurnal tide and thermospheric heat sources on the formation temperature inversion layers, Geophys. Res. Lett., 25, 1483–1486.

Thayaparan, T., Hocking, W. K., and MacDougall, J.: Observational evidence of gravity wave-tidal interactions using the UWO 2 MHz radar, Geophys. Res. Lett., 22, 381–384, 1995.

Tsuda, T., Nishida, M., Rocken, C., and Ware, R. H.: A global morphology of gravity wave activity in the stratosphere revealed by the GPS occulatation data (GPS/MET), J. Geophys. Res., 105, 7257–7273, 2000.

Whiteway, J., Carswell, A. I., and Ward, W. E.: Mesospheric temperature inversions with overlaying nearly adiabatic lapse rate: An indication of well-mixed turbulent layer, Geophys. Res. Lett., 22, 1201–1204, 1995.